Enhancing anticancer, antioxidant, and antibacterial activities of chalcogen-based SnSe nanoparticles synthesized through the co-precipitation method

H. A. Rather [1*], J. B. A. Wahid [2], M. A. Dar [3], L. Guganathan [4], U. A. Dar [5], P. Arularasan [6], S. E. I. Yagoub [7], L. G. Amin [7]

[1]*Department of Basic Science, Faculty of Science and Technology, Kampala International University, Uganda.*

[2]*Medical Laboratory Technology, Faculty of Applied Medical Sciences, Northern Border University, Arar 73213, Saudi Arabia*

[3]*Faculty of Allied Health Sciences, Chettinad Hospital, and Research Institute, Chettinad Academy of Research and Education, Kelambakkam-603103, Tamil Nadu, India*

[4]*Department of Physics, Saveetha School of Engineering, Saveetha Institute of Medical and Technical Science (SIMATS), Thandalam, Chennai- 602105*

[5]*Key laboratory of biobased polymer materials, College of Polymer Science and Engineering, Qingdao University of Science and Technology, Qingdao-266042, China*

[6]*Post Graduate Department of Physics, Dwaraka Doss Goverdhan Doss Vaishnav College, University of Madras, Chennai-600106, Tamil Nadu, India*

[7]*Physics Department, Faculty of Science, Northern Border University, Arar, Saudi Arabia.*

SnSe powdered nanoparticles (NPs) are prepared using the co-precipitation method. The powdered NPs were studied using X-ray diffraction (XRD), UV-absorbance spectroscopy, and scanning electron microscopy (SEM) characterization techniques. The XRD result indicates that NPs are orthorhombic with a crystalline size of 4 nm for TS-1, 6 nm for TS-2, and 13 nm for TS-3, respectively. The SEM images show the surface morphology of the prepared NPs is not fully spherical, but semi-flower-like. The optical properties of the powdered NPs are found by UV-Vis absorbance spectroscopy, in which the highest absorbance was found between 200 nm and 300 nm. The anticancer activities of SnSe NPs against HELA (Cervical cancer cell line) and HEK (Human embryonic kidney cell line) increase with the Se ratio, which indicates that Se tends to enhance anticancer activities. The DPPH (1, 1-diphenyl-2-picrylhydrozyl), metal chelating, and lipid peroxidation activities show a similar trend of increasing percentage with the increasing Se ratio. The antibacterial activity was carried out against two Gram-negative bacteria, *Escherichia coli*, and *Klebsiella pneumoniae,* and two Gram-positive bacteria, *Streptococcus pneumonia*, and *Streptococcus epidermidis* possess a better antibacterial effect.

(Received January 24, 2025; Accepted May 7, 2025)

Keywords: HELA, HEK, DPPH, Gram-negative, Gram-positive

1. Introduction

Metal chalcogenides, including compounds such as SnSe, have garnered significant attention in biological applications due to their unique structural, electronic, and physicochemical properties. SnSe, a two-dimensional layered material, exhibits exceptional thermoelectric performance, high chemical stability, and a low degree of toxicity, making it a promising candidate for diverse bio-related applications [1]. SnSe NPs are being explored for their biocompatibility and ability to act as carriers for therapeutic agents. They can be functionalized with targeting molecules

* Corresponding authors: hhiillaallbiotech@gmail.com
https://doi.org/10.15251/CL.2025.225.461

to achieve controlled and site-specific drug release, thereby enhancing treatment efficacy and reducing side effects. Moreover, the antibacterial and antifungal properties of SnSe have been demonstrated in several studies, making it useful for creating antimicrobial coatings for medical devices, implants, and wound dressings [2, 3]. These coatings can significantly reduce the risk of infections associated with medical procedures. SnSe-based materials support anticancer activities, due to their mechanical flexibility and bioactive properties, and provide an excellent environment for cell growth and differentiation, aiding the regeneration of damaged tissues such as bone, cartilage, or skin. The material's ability to promote the adsorption of proteins and cell adhesion further enhances its suitability for such applications [4].

Additionally, the intrinsic thermoelectric properties of SnSe open up possibilities for developing self-powered implantable medical devices that can harvest energy from the body's natural temperature gradients, eliminating the need for external power sources. Despite these advantages, challenges such as scalability, cost-effectiveness, and potential long-term biocompatibility issues need to be addressed to fully realize the potential of SnSe in biological applications [5,6]. Advances in nanotechnology and surface engineering are expected to play a pivotal role in overcoming these barriers, enabling broader adoption in the biomedical field. As research continues to unravel the capabilities of SnSe and other metal chalcogenides, these materials are poised to revolutionize the intersection of nanotechnology and medicine, offering innovative solutions for diagnostics, therapeutics, and regenerative medicine [7-9]. Due to these biomedical applications, herein SnSe materials are synthesized through the precipitation method in three different concentrations and utilized for biological applications. The SnSe NPs have been investigated and reported for their anti-bacterial activity against several species, including *E. coli, S. aureus,* and *T. viridis*. The anticancer activities of SnSe NPs are taken against HELA (Cervical cancer cell line) and HEK (Human embryonic kidney cell line). Further, the SnSe NPs are tested against DPPH (1, 1-diphenyl-2-picrylhydrozyl), metal chelating and lipid peroxidation antioxidant activities.

2. Experimental details

Tin (II) chloride ($Sncl_2.2H_2O$), selenium powder (Se), sodium hydroxide from Sigma-Aldrich 98% purity, and deionized water are the ingredients needed to synthesize tin selenide NPs. All of the above compounds are used without additional purification. Firstly, take 100 ml of deionized water in a beaker. Put 2.24 g of $SnCl_2.2H_2O$ stirrer continuously by adding NaOH pellets frequently until the solution becomes transparent (Solution A). Take a second beaker add 2.2 0g of SnO_2 in 100 ml of deionized water stir continuously and add 1.34 g of $NaBH_4$ tablets under stirring conditions until the solution becomes transparent (Solution B). Finally, add solution A to solution B by burette dropwise under stirring conditions for 15 minutes then precipitation was obtained and settled down at the bottom of the beaker. The final precipitation obtained is dried in an oven for 6 hours at 100 ºC and finally, the powder was named TS-1 NPs. A similar procedure was followed for TS-2 (1:2) and TS-3 (1:3) NP samples. The characterization techniques and the sample preparation for antioxidant activities such as DPPH radical scavenging activity, lipid peroxidation, metal chelating activity and anticancer activity were similar to our previous report [10-14].

3. Results and discussions

3.1. Synthesis and characterization of SnSe chalcogenides

Figure 1a shows the XRD pattern of TS-1, TS-2 and TS-3 NPs, which demonstrate the creation of an orthorhombic crystal structure and the peaks are indexed as (201), (111), (411), (501), (220), (610), (502), (512) and (620) at the angular positions of 26.9°, 31.6°, 43.6°, 44.4°, 45.4°, 51.7°, 56.1°,64.3° and 66.7°, confirmed from JCPDS card no: 89-0234. The XRD graph shows no undesirable phase that does not react and match with any structure, verifying the material's purity. All of the diffraction peaks correspond to the XRD peaks identified from the earlier research for SnSe chemical precipitation [15]. The strength of the peak in the TS-1 diffractogram corresponding

to [111] at 31° was observed to rise with increasing Sn concentration and was found to be shifting toward the left as shown in Figure 1b, due to lattice expansion [16,17]. The following formulae are used to compute the other parameters:

$$D = \frac{K\lambda}{\beta cos\theta} \quad (1)$$

The calculated values for TS-1, TS-2, and TS-3 NPs reveal crystalline sizes ranging from 4 to 13 nm in diameter.

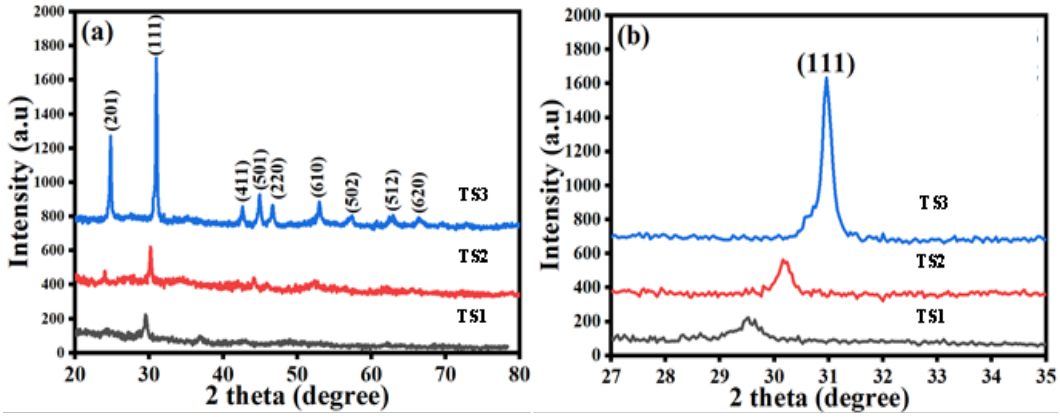

Fig. 1. (a) XRD spectra of TS-1. TS-2 and TS-3 NPs, respectively; (b) Highest intensity peak pattern of TS-1, TS-2 and TS-3 NPs, respectively.

Figure 2 (a - d) indicates the SEM study of TS-3 NPs. The SEM pictures show that the particles are agglomerated cubical shapes attached to small spheres. The spheres connected with the cubical structures make them suitable for biological applications. The optical characteristics of TS-1, TS-2, and TS-3 NPs were investigated using a UV-Vis spectrophotometer.

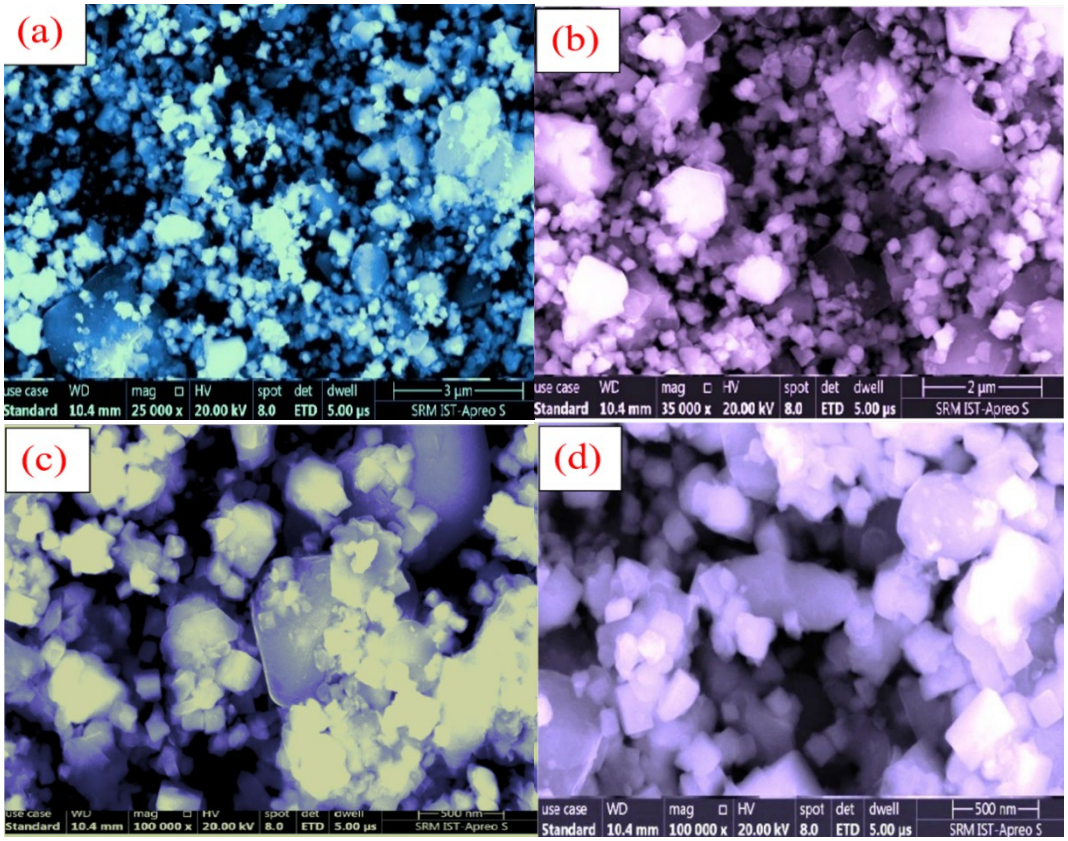

Fig. 2. (a-d): SEM images of TS-3 NPs.

Figure 3 (a & b) depicts the UV-absorbance spectra and transmittance spectra of TS-1, TS-2 and TS-3 NPs. The highest absorbance is seen between 200 nm and 300 nm [18]. For TS-1 highest absorbance was found 239 cm^{-1} and for TS-2 and TS-3 it was found to be 234 and 233 (cm^{-1}).

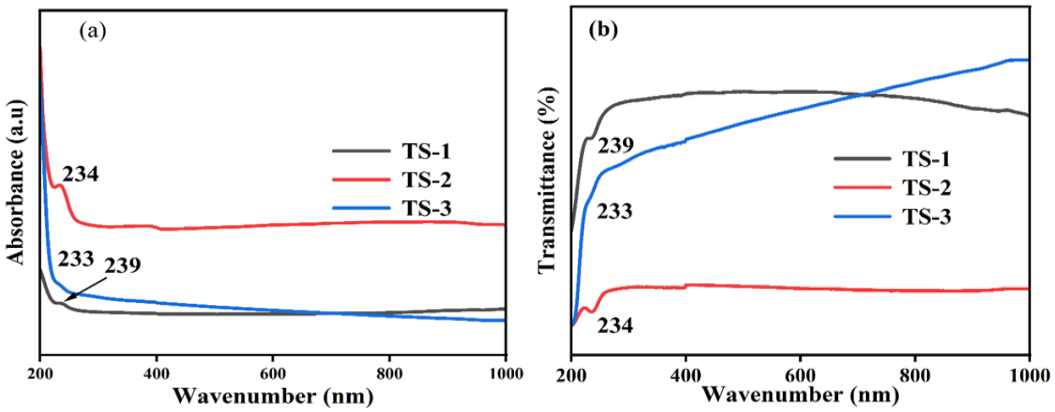

Fig. 3. (a) UV-Absorbance spectra of TS-1, TS-2 and TS-3 NPs, respectively; (*b) UV-transmittance spectra of TS-1, TS-2 and TS-3 NPs, respectively.*

3.1.2. Biological studies

The anticancer activities of TS-1, TS-2 and TS-3 NPs were carried out against two cell lines viz, HEK293 cells (human embryonic kidney cell line) and HELA (cervical cancer line). Figure 4 (a, b) shows the cell proliferation inhibition percentage of HEK293 cell line and HELA cell line of

pure TS-1, TS-2 and SnSe-NPs, respectively. The cell proliferation inhibition percentage of HEK293 cell line and HELA cell line increases TS-1, TS-2 and SnSe-NPs. The proliferation inhibition of TS-1, TS-2 and TS-3 against HEK293 cell line was 22%, 24% and 37%, respectively. The proliferation inhibition of TS-1, TS-2 and TS-3 against HELA cell line was 10%, 25% and 35%, respectively. This determines the TS-3 NPs show better cell proliferation inhibition percentage than TS-2 and TS-3 NPs. The factors that are responsible for increasing the efficiency of anticancer activities of pure TS-1, TS-2 and TS-3 are energy bandgap, small crystalline size and clear agglomerated spherical morphology in nanoparticle range shown in SEM images.

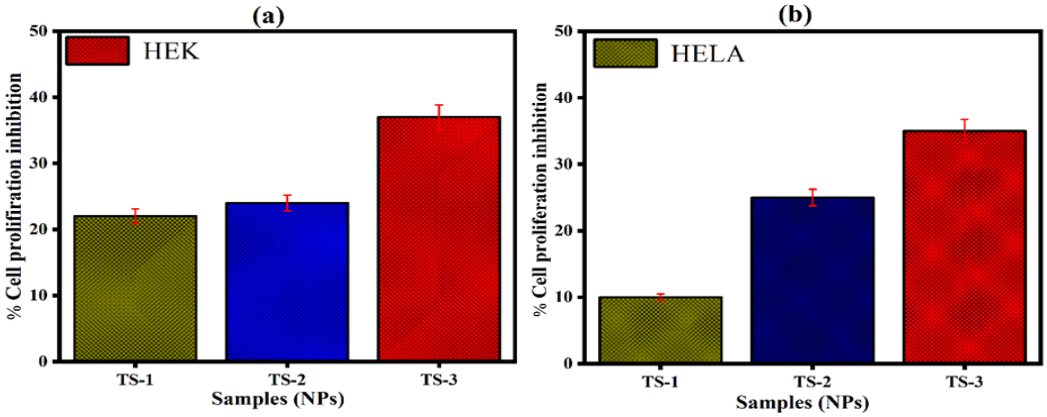

Fig. 4. (a) Cell proliferation inhibition percentage of HEK293 cell line; (b) Cell proliferation inhibition percentage of HELA cell line of TS-1, TS-2 and TS-3, respectively.

The antioxidant activity of TS-1, TS-2 and TS-3 NPs can be evaluated by estimating DPPH, metal chelating and lipid peroxidation assays. Figure 5(a) represents DPPH scavenging activity of TS-1, TS-2 and TS-3 NPs. From Figure 5(a), it is observed that the free radical scavenging activity of TS-1, TS-2 and TS-3 NPs increased from sample SnS-1 to TS-3. . Figure 5(b) represents the lipid peroxidation activity of TS-1, TS-2 and TS-3 NPs. Here, it is also observed from Figure 5b, that the lipid peroxidation scavenging activity increases from TS-1, TS-2 and TS-3 NPs. Figure 5(c) represents the metal chelating activity of TS-1, TS-2 and TS-3 NPs, respectively. Similarly, the scavenging activity of lipid peroxidation activity increases from TS-1 to TS-3 NPs determining that increasing the ration of Se powder has great impact on the scavenging percentage of lipid peroxidation. The free radical scavenging activity of TS-1, TS-2 and TS-3 NPs is a surface reaction that depends only on the surface that comes in contact with the free radicals. This percentage of radical scavenging activity depends on various factors such as morphology, particle size, defects etc [19]. Previous reports suggest that the antioxidant activities of Sn-based NPs increase due to different reasons. Kumari etal., synthesized SnO_2 NPs by using *Punica granatum* leaf extract and antioxidant activity increases with the increase in sample dosage [20]. Vidu et al., reported similar results with increasing the concentration of SnO_2 NPs, the radical scavenging activity increases [21]. Khan et al., enhanced antioxidant activity of un-doped SnO_2 and Co-doped SnO_2 NPs synthesized by using Clerodendrum inerme with increasing in concentration of samples from 25 to 100 μgmL^{-1} [22].

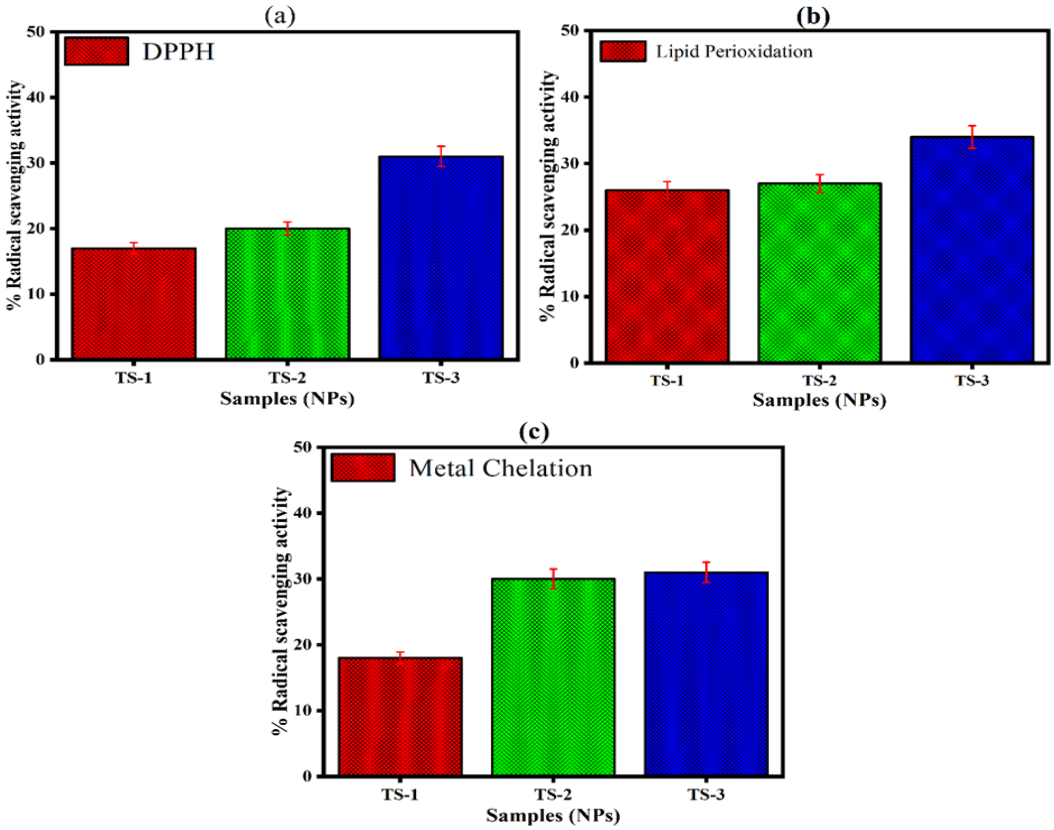

Fig. 5. (a) DPPH scavenging activity; (b) lipid peroxidation activity; (c) Metal chelating activity TS-1, TS-2 and TS-3 NPs, respectively.

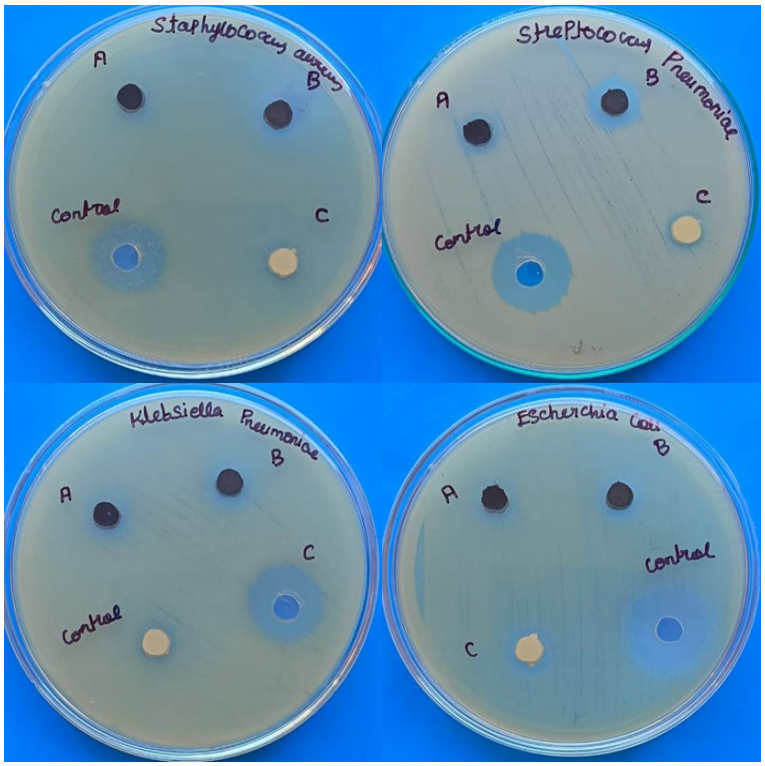

Fig. 6. Antibacterial activity of TS-1, TS-2 and TS-3 NPs against S. Aureus, S. Pneumoniae, K. pneumoniae and E. coli bacteria strains.

The antibacterial activities of TS-1 (coded as A), TS-2 (coded as B) and TS-3 (coded as C) NPs with a concentration 100 µg/ml was done against four pathogenic bacterial strains i.e., *Staphylococcus aureus*, *Staphylococcus pneumonia* (Gram-positive) and *Klebsiella pneumonia, Escherichia coli,* (Gram-negative) shown in the Figure 6 and zone of inhibition is represented in bar diagram (Figure 7). From Table 1, it was observed that the mean zone of inhibition acquired by TS-1 (coded as A), TS-2 (coded as B) and TS-3 (coded as C) NPs is in the range of 9 -14 mm in all bacteria pathogens. In comparison, the highest was shown in *Escherichia coli* (14 mm) for TS-3 NPs and *Staphylococcus aureus*, *Staphylococcus pneumonia* (Gram-positive) and *Klebsiella pneumonia, Escherichia coli,* (Gram-negative) shows (12 mm) for TS-2 (coded as B) at 100µg/mL. The results demonstrated that increasing Se content host material was positively inducing the bactericidal property of SnSe NPs. Metal oxide NPs, on the other hand, have several potential modes of action against bacteria, including electrostatic contact, breakdown of NPs with microbial cell walls, and production of reactive oxygen species (ROS) in response to light energy [23-25].

Table 1. Zone of inhibition of the TS-1 (A), TS-2 (B), and TS-3 (C) NPs against S. Aureus, S. Pneumoniae, K. Pneumoniae, and E. coli bacteria strains.

Bacterial pathogens	Zone of inhibition mm			
	A	**B**	**C**	**Positive**
Staphylococcus aureus	-	11	9	20
Streptococcus pneumoniae	10	11	10	22
Klebsiella pneumoniae	9	10	-	20
Escherichia coli	10	11	14	22

4. Conclusion

SnSe nanoparticles were successfully synthesized via the Co-precipitation technique and comprehensively characterized using XRD, SEM, and UV-absorbance spectroscopy. The SEM images revealed a distinctive flower-like morphology. Optical characteristics, examined through UV-absorbance spectroscopy, indicated the highest absorbance between 200 nm and 300 nm. The scavenging percentage of HELA, HEK, DPPH, lipid peroxidation and metal chelating activity increases with concentration Se from 1 to 3 ratios, respectively. The SnSe NPs shows better antimicrobial activity against all four microbial pathogens bacteria's (i.e., two Gram-negative bacteria like *Escherichia coli*, *Klebsiella pneumoniae* and two Gram-positive bacteria like *Streptococcus pneumonia*, *Streptococcus epidermidis*).

Acknowledgments

The authors thank the Deanship of Scientific Research at Northern Border University, Arar, KSA, for funding this research work through the project number "NBU-FFR-2025-1329-15".

Declaration

The authors declare no competing interests.

References

[1] S. Patai, Z. Rappaport, The Chemistry of Triple Bonded Functional Groups, The Chemistry of Organic Selenium and Tellurium Compounds, 192 (1978).

[2] J. Ling, Y. Chang, Z. Yuan, Q. Chen, L. He, T. Chen, ACS Appl. Mater. Interfaces, 14, 27651-27665 (2022); https://doi.org/10.1021/acsami.2c05533

[3] M. Gao, Z. Wang, H. Zheng, L. Wang, S. Xu, X. Liu, W. Li, Y. Pan, W. Wang, X. Cai, et al., Angew. Chem. Int. Ed. Engl., 59, 3618-3623 (2020); https://doi.org/10.1002/anie.201913035

[4] H. Dai, Q. Fan, C. Wang, Exploration, (2022).

[5] D. Wu, J. Li, S. Xu, Q. Xie, Y. Pan, X. Liu, R. Ma, H. Zheng, M. Gao, W. Wang, et al., J. Am. Chem. Soc., 142, 19602-19610 (2020); https://doi.org/10.1021/jacs.0c08360

[6] M. Gao, X. Liu, Z. Wang, H. Wang, T. Asset, D. Wu, J. Jiang, Q. Xie, S. Xu, X. Cai, et al., Nano Today, 44, 101456 (2022); https://doi.org/10.1016/j.nantod.2022.101456

[7] F. Li, H. Wang, R. Huang, W. Chen, H. Zhang, Adv. Funct. Mater., 32, 2200516 (2022); https://doi.org/10.1002/adfm.202200516

[8] A.U. Ahmad, H. Liang, S. Ali, G. Dastgeer, Q. Abbas, A. Farid, A. Abbas, A. Idrees, M. Iqbal, Z. Farooq, Ceram. Int., 46, 7298-7305 (2020); https://doi.org/10.1016/j.ceramint.2019.11.224

[9] D. Zhang, Z. Tang, H. Huang, G. Zhou, C. Cui, Y. Weng, W. Liu, S. Kim, S. Lee, M. Perez-Neut, et al., Nature, 574, 575-580 (2019); https://doi.org/10.1038/s41586-019-1678-1

[10] B.A. Ashwar, A. Gani, I.A. Wani, A. Shah, F.A. Masoodi, D.C. Saxena, Food Hydrocoll., 56, 108-117 (2017); https://doi.org/10.1016/j.foodhyd.2015.12.004

[11] A. Shah, F.A. Masoodi, A. Gani, B.A. Ashwar, Radiat. Phys. Chem., 117, 120-127 (2015); https://doi.org/10.1016/j.radphyschem.2015.06.022

[12] N. Noor, A. Gani, F. Jhan, J.L.H. Jenno, M.A. Dar, Ultrasonics Sonochemistry, 76, 105655 (2021); https://doi.org/10.1016/j.ultsonch.2021.105655

[13] T.A. Dar, B. Thirunavukkarasu, A. Ganapathi, J.W. Jebaraj, Materials Today: Proceedings, 59, 352-356 (2022); https://doi.org/10.1016/j.matpr.2021.11.204

[14] M.A. Dar, N.A. Mala, G.N. Dar, S.S. Kumar, D. Govindarajan, Adv. Nat. Sci.: Nanoscience and Nanotechnology, 11(4), 045001 (2020); https://doi.org/10.1088/2043-6254/abb36a

[15] X.F. Wang, B. Liu, Q.Y. Xiang, Q.F. Wang, X.J. Hou, D. Chen, G.Z. Shen, J. Chem. Sus.Chem., 7, 308-313 (2014); https://doi.org/10.1002/cssc.201300241

[16] B. Pejova, I. Grozdanov, Thin Solid Films, 515, 5203-5211 (2007); https://doi.org/10.1016/j.tsf.2006.11.016

[17] N. Karamat, M.N. Ashiq, F.M. Ehsan, S. Ijaz, I. Ali, H.I. Gul, J. Alloys Compd., 689, 94-106 (2016); https://doi.org/10.1016/j.jallcom.2016.07.260

[18] L. Das, A. Guleria, S. Adhikari, RSC Adv., 5, 61390-61397 (2015); https://doi.org/10.1039/C5RA09448H

[19] V.K. Vidhu, D. Philip, Spectrochim. Acta Part A: Mol. Biomol. Spectrosc., 134, 372-379 (2015); https://doi.org/10.1016/j.saa.2014.06.131

[20] M.M. Kumari, D. Philip, Powder Technol., 270, 312-319 (2015); https://doi.org/10.1016/j.powtec.2014.10.034

[21] V.K. Vidhu, D. Philip, Spectrochim. Acta Part A, 134, 372-379 (2015); https://doi.org/10.1016/j.saa.2014.06.131

[22] S.A. Khan, S. Kanwal, K. Rizwan, S. Shahid, Microb. Pathogenesis, 125, 366-384 (2018); https://doi.org/10.1016/j.micpath.2018.09.041

[23] L. Zhang, Y. Ding, M. Povey, D. York, Prog. Nat. Sci., 18, 939-944 (2008); https://doi.org/10.1016/j.pnsc.2008.01.026

[24] R. Jalal, E.K. Goharshadi, M. Abareshi, M. Moosavi, A. Yousefi, P. Nancarrow, Mater. Chem. Phys., 121, 198-201 (2010); https://doi.org/10.1016/j.matchemphys.2010.01.020

[25] K. Kasemets, A. Ivask, H.-C. Dubourguier, A. Kahru, Toxicol. In Vitro, 23, 1116-1122 (2009); https://doi.org/10.1016/j.tiv.2009.05.015